GLIA

WILEY

RESEARCH ARTICLE

Amyloid-β impairs the phagocytosis of dystrophic synapses by astrocytes in Alzheimer's disease

Maria V. Sanchez-Mico[1,2,3,7] | Sebastian Jimenez[1,2,3] | Angela Gomez-Arboledas[3,4] | Clara Muñoz-Castro[1,2,3] | Carmen Romero-Molina[1,2,3] | Victoria Navarro[1,2,3] | Elisabeth Sanchez-Mejias[3,4] | Cristina Nuñez-Diaz[3,4] | Raquel Sanchez-Varo[3,4] | Elena Galea[5,6] | José C. Davila[3,4] | Marisa Vizuete[1,2,3] | Antonia Gutierrez[3,4] | Javier Vitorica[1,2,3]

[1]Dpto. Bioquimica y Biologia Molecular, Facultad de Farmacia, Universidad de Sevilla, Sevilla, Spain

[2]Instituto de Biomedicina de Sevilla (IBiS)-Hospital Universitario Virgen del Rocío/CSIC/Universidad de Sevilla, Sevilla, Spain

[3]Centro de Investigacion Biomedica en Red sobre Enfermedades Neurodegenerativas (CIBERNED), Madrid, Spain

[4]Dpto. Biologia Celular, Genetica y Fisiologia, Instituto de Investigación Biomedica de Malaga-IBIMA, Facultad de Ciencias, Universidad de Malaga, Malaga, Spain

[5]Institut de Neurociències and Departament de Bioquímica i Biologia Molecular, Unitat de Bioquímica de Medicina, Universitat Autònoma de Barcelona, Barcelona, Spain

[6]ICREA, Barcelona, Spain

[7]Department of Neurology, Massachusetts General Hospital and Harvard Medical School, Charlestown, Massachusetts

Correspondence
Antonia Gutierrez, Dpto. Biologia Celular, Genetica y Fisiologia, Facultad de Ciencias, Universidad de Malaga, Campus de Teatinos s/n, Malaga 29071, Spain.
Email: agutierrez@uma.es

Javier Vitorica, Dpto. Bioquimica y Biologia Molecular, Facultad de Farmacia. Universidad de Sevilla, C/Prof. Garcia Gonzalez 2, Sevilla 41012, Spain.
Email: vitorica@us.es

Abstract

Reactive astrocytes and dystrophic neurites, most aberrant presynaptic elements, are found surrounding amyloid-β plaques in Alzheimer's disease (AD). We have previously shown that reactive astrocytes enwrap, phagocytose, and degrade dystrophic synapses in the hippocampus of APP mice and AD patients, but affecting less than 7% of dystrophic neurites, suggesting reduced phagocytic capacity of astrocytes in AD. Here, we aimed to gain insight into the underlying mechanisms by analyzing the capacity of primary astrocyte cultures to phagocytose and degrade isolated synapses (synaptoneurosomes, SNs) from APP (containing dystrophic synapses and amyloid-β peptides), Tau (containing AT8- and AT100-positive phosphorylated Tau) and WT (controls) mice. We found highly reduced phagocytic and degradative capacity of SNs-APP, but not AT8/AT100-positive SNs-Tau, as compared with SNs-WT. The reduced astrocyte phagocytic capacity was verified in hippocampus from 12-month-old APP mice, since only $1.60 \pm 3.81\%$ of peri-plaque astrocytes presented phagocytic structures. This low phagocytic capacity did not depend on microglia-mediated astrocyte reactivity, because removal of microglia from the primary astrocyte cultures abrogated the expression of microglia-dependent genes in astrocytes, but did not affect the phagocytic impairment induced by oligomeric amyloid-β alone. Taken

Antonia Gutierrez and Javier Vitorica are co-senior corresponding authors.

together, our data suggest that amyloid-β, but not hyperphosphorylated Tau, directly impairs the capacity of astrocytes to clear the pathological accumulation of oligomeric amyloid-β, as well as of peri-plaque dystrophic synapses containing amyloid-β, perhaps by reducing the expression of phagocytosis receptors such as Mertk and Megf10, thus increasing neuronal damage in AD. Therefore, the potentiation or recovery of astrocytic phagocytosis may be a novel therapeutic avenue in AD.

1 | INTRODUCTION

Alzheimer's disease (AD), the most common cause of dementia in the elderly, is pathologically characterized by the accumulation of extracellular amyloid-β (Abeta) plaques (Hane, Lee, & Leonenko, 2017; Masters et al., 1985), intraneuronal hyperphosphorylated Tau-laden neurofibrillary tangles (Laurent, Buée, & Blum, 2018; Spillantini & Goedert, 2013), synaptic loss and neuronal degeneration (Forner, Baglietto-Vargas, Martini, Trujillo-Estrada, & LaFerla, 2017; Hane et al., 2017), and presence of reactive microglia and astrocytes (Dansokho & Heneka, 2018; Heneka et al., 2015; Liu, Cui, Zhu, Kang, & Guo, 2014; Zhang & Jiang, 2015). In particular, astrocytes surrounding Abeta plaques show increase in GFAP, vimentin, and BLBP expression, and increase in the occupied area and cell hypertrophy (Gomez-Arboledas et al., 2018). Astrocyte reactivity or astrogliosis, as measured with GFAP expression, progresses along with Abeta and Tau pathologies in transgenic mouse models and AD patients (Olabarria, Noristani, Verkhratsky, & Rodríguez, 2010; Osborn, Kamphuis, Wadman, & Hol, 2016; Perez-Nievas & Serrano-Pozo, 2018; Rodríguez, Olabarria, Chvatal, & Verkhratsky, 2009; Verkhratsky, Zorec, Rodríguez, & Parpura, 2016). However, it is not clear whether this response exacerbates or attenuates AD pathology, or is a consequence of the disease with little pathological bearing.

An important feature observed in the brain of AD patients and amyloidogenic mice is the early appearance of dystrophic neurites close to Abeta plaques. Dystrophic neurites, highly swollen axonal/presynaptic elements, significantly contribute to synaptic and neuronal pathology in preclinical stages of AD (Nixon, 2007; Nixon & Yang, 2011; Sanchez-Varo et al., 2012; Torres et al., 2012). Furthermore, neuritic plaques are surrounded by reactive microglia and astrocytes (Heneka et al., 2015; Meyer-Luehmann et al., 2008; Serrano-Pozo, Betensky, Frosch, & Hyman, 2016), but it is not clear whether astrocytes promote the development and progression of dystrophies or whether, on the contrary, they constitute a physical barrier to limit their growth and protect other cells from the toxicity on the plaque halo, as suggested by several authors (Kraft et al., 2013; Perez-Nievas & Serrano-Pozo, 2018), and are engaged in the phagocytosis of dystrophies. The latter scenario is supported by evidence that astrocytes can phagocytose Abeta (Jones, Minogue, Connor, & Lynch, 2013; Wyss-Coray et al., 2003; Xiao et al., 2014) and synapses (Chung et al., 2013; Chung, Allen, & Eroglu, 2015; Clarke & Barres, 2013), which may represent an attempt to protect other cells, such that alterations in the phagocytic capacity of astrocytes may result in reduced clearance of Abeta and dystrophic synapses. Previously, we demonstrated that astrocytes are capable to enwrap, internalize, and degrade presynaptic dystrophies in the hippocampus of APP mice and AD patients (Gomez-Arboledas et al., 2018). However, the proportion of engulfed dystrophic neurites by astrocytes was below 7% of total dystrophies. This fact, along with the accumulation of these dystrophies during the disease course, suggests that the efficiency of the astrocyte phagocytic process might be limited or impaired. Reduced clearance of accumulated dystrophic neurites may contribute to the progression of the AD pathology. In this study, we have examined the phagocytic capacity of astrocytes using synaptoneurosomes (SNs) isolated from APP transgenic mice, which contain dystrophic synapses, compared to those isolated from WT and Tau (P301S) mice, which do not present dystrophic neurites. Impaired phagocytosis was observed in the presence of SNs from APP, but not from Tau mice. Finally, the maintenance of the phagocytic impairment after microglia depletion supports the conclusion that Abeta, and not microglia-released factors, is the factor limiting phagocytosis in astrocytes in AD.

2 | MATERIALS AND METHODS

2.1 | Transgenic mouse models

APP751$_{sl}$ and Tau-P301S transgenic mice were used. The APP mice (Blanchard et al., 2003) over-expressed the human mutant APP751 (under Thy-1 promoter) carrying the Swedish (KM670/671NL) and London (V717I) mutations. The Tau-P301S mice (Jackson Lab) (Romero-Molina et al., 2018; Yoshiyama et al., 2007) expressed human 4-repeat 1 N-terminal insert tau with P301S mutation driven by the mouse prion protein (Prnp) promoter (B6;C3-Tg(Prnp-MAPT*P301S)PS19Vle/J). Non-transgenic mice (WT) of the same genetic background (C57/BL6) and age were used as controls. In this study we used 3- and 12-month-old APP mice or 9-month-old Tau-P301S model. Animal experiments were performed in accordance with the Spanish and the European Union regulations (RD53/2013 and 2010/63/UE) with the approval of the Animal Research Committees from the Universities of Seville and Malaga (Spain).

2.2 | Synaptoneurosomes preparation

Synaptoneurosomes were isolated as described previously (Puighermanal, Biever, & Valjent, 2016) with some modifications. Briefly, brain hemicortices were gently homogenized with a glass Dounce homogenizer, in 1 ml of cold SN-Buffer ($CaCl_2$ 2.5 mM, NaCl 124 mM, KCl 3.2 mM, KH_2PO_4 1.06 mM, $NaHCO_3$ 26 mM, $MgCl_2$ 1.3 mM, D(+)Glucose 10 mM and HEPES 20 mM, pH 7.4). The homogenate was sequentially filtered by three Nylon 100 μm filters (Millipore) and one Miltex 10 μm filter (Millipore) and the filtrate was centrifuged (at 4,000g, 1 min at 4°C). The supernatant was then centrifuged at 14,000g (5 min at 4°C). The final pellet was resuspended in 300 μl SN-Buffer and kept at 4°C.

2.3 | Preparation of soluble fractions (S1)

Soluble fractions (S1) were prepared from mouse brain cortex as previously described (Jimenez et al., 2014). Briefly, mouse tissue was homogenized using Dounce's homogenizer, in TBS (20 mM Tris–HCl, 140 mM NaCl, pH 7.5) plus protease and phosphatase inhibitors (Roche). Homogenates were ultracentrifuged at 100,000g (4°C for 60 min, OptimaMAX Preparative Ultracentrifuge, Beckman Coulter). Supernatants, which comprise both extracellular and cytosolic proteins (S1 fractions), were aliquoted and stored at −80°C until use.

2.4 | Cell cultures

Primary astrocyte cell cultures were performed as previously described (Jimenez et al., 2008). Briefly, dissected P3 newborn WT cortices were treated with trypsin-EDTA (Biowest) for 5 min. The treatment was stopped using complete DMEM-F12 plus 10% FBS and the cells were mechanically dissociated. After mechanical dissociation, the debris was eliminated by filtration (40 μm; BD Falcon) and the cells were seeded on poly-D-lysine (Sigma-Aldrich) treated Nunc 24-well plates. The cells were grown (37°C and 5% CO_2) in DMEM-F12, 2 mM glutamine, 10% (v/v) fetal bovine serum, non-essential amino acids (1×), plus gentamycin (10 μg/ml), penicillin (100 U/ml) and streptomycin (100 μg/ml) (all from Biowest). The medium was replaced every 4 days. After 20–25 days in culture, the mixed glial cultures were treated with DMEM-F12 and Trypsin 0.25%-EDTA (3:1 v/v) for 30 min. The treatment was stopped using the same growth media and the supernatant was collected, centrifuged (800g, 5 min) and astrocytes were seeded on new poly-D-lysine treated Nunc 24-well plates. Astrocytes were grown (37°C and 5% CO_2) in the same media. For the complete elimination of microglia, the cultures were treated (3 days) with Clodronate liposomes (100 μg/ml; Liposoma Research Liposomes) as described (Kumamaru et al., 2012). WJE astrocytes (Morikawa et al., 2005) were grown (37°C and 5% CO_2) in DMEM/F-12 w/o ʟ-Glutamine with fetal bovine serum (10%), penicillin (100 U/ml), streptomycin (100 μg/ml), sodium pyruvate (1%) and geneticin (200 μg/ml) (all from Biowest).

Primary microglial cultures were prepared as described (Jimenez et al., 2008). Briefly, mixed astrocytic/microglial cultures were mildly trypsinized as described above and the supernatant (astrocytic fraction) was removed. The attached cells (microglial cells) were cultured in DMEM-F12, 2 mM glutamine, 10% (v/v) fetal bovine serum, non-essential amino acids (1×), plus gentamycin (10 μg/ml), penicillin (100 U/ml) and streptomycin (100 μg/ml) (all from Biowest).

2.5 | Total RNA and protein extraction, reverse transcription and quantitative real-time RT-PCR

Total RNA and proteins were sequentially extracted, from cells or mouse hippocampal tissue, using Tripure Isolation Reagent (Roche) (100 mg tissue/1 ml Tripure Isolation Reagent) following manufacture recommendations (Jimenez et al., 2014; Romero-Molina et al., 2018; Sanchez-Mejias et al., 2016). RNA integrity was determined by RNA Nano 6000 (Agilent) (RIN 8.5 ± 0.5). RNA was quantified using Nanodrop 2000 (Thermo Fischer). Proteins were quantified using Lowry. Reverse transcription (RT) (4 μg of total RNA as template) was performed with High Capacity cDNA Archive Kit (Applied Biosystems). For real time qPCR, 40 ng of cDNA were mixed with 2× Taqman Universal Master Mix (Applied Biosystems) and 20× Taqman Gene Expression assay probes (Applied Biosystems). Quantitative RT-PCR (qPCR) was done using Taqman probes (Applied Biosystems), unless specifically stated. The different cDNAs were mixed with Taqman Universal Master Mix (Applied Biosystems) and Taqman Gene Expression assay probes. The quantitative PCR reactions (qPCR) were done using an ABI Prism 7900HT (Applied Biosystems). Results were always expressed using the comparative double-delta Ct method ($2^{-\Delta\Delta Ct}$). ΔCt values represent GAPDH normalized expression levels. This normalization approach was validated by retesting the expression of one gene, Mertk, with three different housekeeper genes, GAPDH, beta-actin and 18S. The results were identical using all three housekeeper genes (not shown).

To assess microglia dependent- or independent gene expression, primer sequences were obtained from Liddelow et al., 2017 and qPCR was done using FastStart Universal SYBR Green Master (Roche).

2.6 | Western blot and dot blot

Western blots and dot blots were done as previously described (Jimenez et al., 2008; Romero-Molina et al., 2018; Sanchez-Mejias et al., 2016). For western blots, samples were loaded onto either 12% SDS-Tris–Glycine-PAGE or 4–20% precast gel gradient (BioRad). Proteins were then transferred to nitrocellulose membranes (Optitran, GE Healthcare Life Sciences) or PVDF for Abeta peptides (Millipore). Membranes were blocked, using 5% low-fat milk in TPBS (0.1% Tween-20, 137 mM NaCl, 2.7 mM KCl, 10 mM phosphate buffer, pH 7.4) and incubated (overnight at 4°C) with the appropriate primary antibody. The following primary antibodies were used: anti-phospho-tau AT100 (pSer212/Thr214, mouse monoclonal antibody 1:1000, Thermo Fisher Scientific), AT8 (pSer202/Thr205, mouse monoclonal antibody 1:1000, Thermo Fisher Scientific); anti-total tau Tau46 (mouse monoclonal antibody 1:000 Cell Signaling Technology); Tau12 (mouse monoclonal antibody 1:10000,

Merck-Millipore); anti-Abeta peptide (mouse monoclonal antibody clone 6E10, 1:6000, Palex, plus mouse monoclonal antibody clone 82E1, 1:6000, IBL); anti-PSD95 (rabbit polyclonal, 1:1000, Cell Signalling); anti-synaptophysin (rabbit polyclonal, 1:1000, Synaptic Systems); anti-VGLUT (rabbit polyclonal, 1:1000, Synaptic Systems); anti-GFAP (mouse monoclonal, 1:5000, Sigma-Aldrich). Membranes were then incubated with the appropriate secondary HRP-conjugated antibody (1:10.000, Cell Signaling). The blots were visualized using the Pierce ECL 2 Western Blotting Substrate detection method (0.5 pg, lower limit sensitivity; Thermo Scientific). The images were obtained and analyzed with ChemiDoc™ Touch Imaging System (Bio-Rad).

For dot blot, 0.1 μg of protein from the different soluble fractions was directly applied to dry nitrocellulose, in a final volume of 3 μl. Then, blots were blocked for 1 h and incubated overnight at 4°C, with anti-Amyloid fibrils (OC, rabbit, 1:5000, Merck-Millipore), anti-prefibrillar oligomers (A11, rabbit, 1:5000 InvitroGen) or GAPDH (rabbit, 1:10000, Cell Signalling) primary antibodies. After incubation, the blots were washed and visualized as described above.

2.7 | Phagocytosis of synaptoneurosomes (TAMRA assay)

SNs were first loaded with 5 μM TAMRA-ester (5-(and-6)-carboxytetramethylrhodamine succinimidyl ester; Sigma-Aldrich) for 2 hr at RT. After loading, free TAMRA-ester was removed by centrifugation and TAMRA-loaded SNs were resuspended in SN-buffer and added (3 μl) to the primary astrocyte culture (1 ml culture media). Primary astrocytes were then incubated for different times (ranging from 0 to 12 hr), gently trypsinized and TAMRA-positive cells identified by Flow Cytometry (λ_{ex} = 492 nm; λ_{em} = 517 nm, LRS II Fortessa; Becton Dickinson).

2.8 | Degradation of synaptoneurosomes (pHRodo chase)

SNs were covalently labeled using 0.3 μM pHRodo (pHrodo™ Red succinimidyl (NHS) ester; Thermo Fisher Scientific) following the manufacturer protocol. Primary astrocytes were incubated for 6 hr with pHRodo-labeled SNs. After this initial incubation, the media were removed and substituted by fresh culture media. Astrocyte cultures were then incubated for different times (0–72 hr after loading), and pHRodo positive cells were identified by flow cytometry (λ_{ex} = 560 nm; λ_{em} = 585 nm) as above. For normalization, the number of pHRodo positive cells at any particular "chase" time was referred to the initial number of phRodo positive cells (6 hr time point).

2.9 | Acridine orange staining

The cellular acidic compartments can be visualized by acridine orange staining. Astrocytes were treated with pHRodo labeled SNs for 6 hours. Cells were incubated with medium containing 0.1 μg/ml

acridine orange (Invitrogen) for 15 min at 37°C. The acridine orange was removed by washing coverslips with PBS and fresh buffer (NaCl 140 mM, KCl 2.5 mM, $MgCl_2$ 1 mM, $CaCl_2$ 2.5 mM, Glucose 10 mM, HEPES 10 mM) was added. Fluorescent images were taken using a confocal microscope (Leica TCS-SP2-AOBS).

2.10 | Immunofluorescence

For double (GFAP/Abeta42) or triple (GFAP/Abeta42/Lamp1) immunofluorescence of primary astrocytes incubated with SNs-APP, cells were seeded onto glass coverslips, fixed with 4% paraformaldehyde in 0.1M phosphate buffer (PB), and then, pre-treated with saline PB (PBS) containing 0.1% Triton X-100 for 12 min and blocked with 1% bovine serum albumin (BSA, Sigma Aldrich) in PBS containing 0.1% Triton X-100 for 1 hr at room temperature. Then, coverslips with astrocytes were sequentially incubated with the selected primary antibodies (anti-GFAP chicken polyclonal antibody, 1:2000 dilution, Merck Millipore; anti-Abeta42 rabbit polyclonal antibody, 1:5000 dilution, Abcam; anti-LAMP1 rat polyclonal antibody, 1:500 dilution, Sigma Aldrich) overnight at room temperature. Cells were then incubated with the corresponding secondary antibody (Alexa Fluor 488, 568 or Cy5, 1:1000 dilution, ThermoFisher) and coverslips were mounted onto gelatin-coated slides with DABCO mounting medium (Sigma Aldrich).

For double immunofluorescence in APP brain sections, mice were anesthetized with sodium pentobarbital (60 mg/kg) and transcardially perfused with 4% paraformaldehyde (PFA), 75 mM lysine, 10 mM sodium metaperiodate in 0.1 M PB (PLP fixative). Fixed and cryoprotected brains were serially sectioned at 40 μm thickness in the coronal plane on a freezing microtome. Sections were sequentially incubated with the selected primary antibodies (anti-GFAP chicken polyclonal antibody, 1:20000 dilution, Millipore; anti-human amyloid precursor protein (APP) rabbit polyclonal antibody, 1:10000 dilution, Sigma Aldrich; anti-Megf10 rabbit polyclonal antibody, 1:1000; Millipore) followed by the corresponding Alexa 488/568 secondary antibodies (1:1000, ThermoFisher). Some immunolabeled GFAP sections were stained with 0.02% thioflavin-S in 50° ethanol. Finally, immunolabeled cultured astrocytes or APP sections were examined under a confocal laser microscope (Leica SP8). Confocal super-resolution images of the Abeta42/lamp1 double immunofluorescence were taken by a SP8 LIGHTNING Confocal microscope (Leica). The specificity of the immune reactions was controlled by omitting the primary antisera.

2.11 | Electron microscopy

For conventional transmission electron microscopy (EM), 250-μm thick sections from 12-month-old APP brains (previously fixed by perfusion with PLP fixative), the coverslips with primary astrocytes (fixed with 4% PFA) and the isolated SNs from 12-month-old APP and age-matched WT mice (fixed with 4% PFA) were postfixed in 1% osmium

tetroxide in 0.1 M PB, block stained with uranyl acetate, dehydrated in graded acetone (brain sections) or ethanol (primary cell cultures and isolated SNs) and embedded in Araldite (EMS, USA) or Durcupan (Sigma Aldrich). For immunogold labeling, 50-µm thick vibratome APP sections or coverslips with primary astrocytes were cryoprotected in a 25% sucrose and 10% glycerol solution, followed by freezing at -80°C in order to increase the antibody binding efficiency. Sections were then incubated 48 h in the primary antibody (anti-Abeta42 rabbit polyclonal antibody, 1:5000 dilution, Abcam; anti-Megf10 rabbit polyclonal antibody 1:1000 dilution, Millipore, or anti-AQP4 rabbit polyclonal antibody, 1:1000 dilution, Sigma Aldrich) in a PBS 0.1M/0.1% sodium azide/2% BSA-solution at 22°C. The tissue-bound primary antibody was detected by the incubation with the corresponding 1.4 nm gold-conjugated secondary antibody (1:100, Nanoprobes) overnight at 22°C. After postfixation with 2% glutaraldehyde and washing with 50 mM sodium citrate, the labeling was enhanced with the HQ Silver™ Kit (Nanoprobes), and gold toned. Finally, the immunolabeled sections were processed as we previously
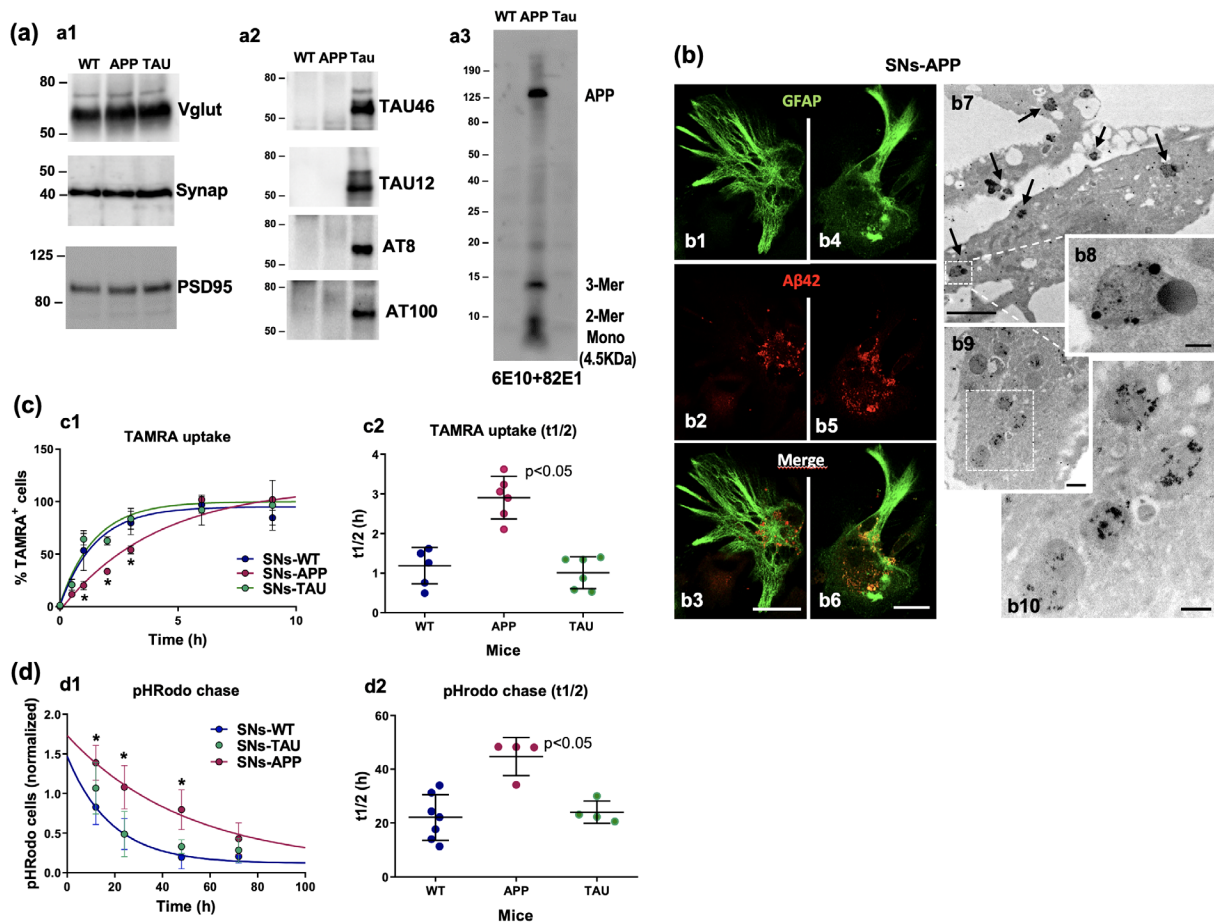

FIGURE 1 Impaired uptake/degradation of APP-derived SNs by astrocytes. (a) Synaptoneurosomes (SNs) isolated from WT, APP (APP751$_{SL}$) or Tau (P301S) mice were analyzed by Western blots. All SNs fractions were clearly positive for pre- and postsynaptic proteins (a1). Total and phosphorylated Tau (a2) were principally detected in Tau-derived SNs whereas Abeta peptides (from monomers to oligomeric forms) were exclusively localized in SNs-APP (a3). B) SNs-APP were phagocytosed by astrocytes in vitro; b1-b6, double GFAP/Abeta42 confocal immunofluorescence revealed the presence of Abeta-positive SNs (in red) within primary astrocytes (in green): b7-b10, Abeta42 immunogold electron microscopy of primary astrocytes incubated with APP-derived SNs displaying multiple Abeta-positive phagosomes in the astrocytic cytoplasm (arrows in b7, and higher magnification details in b8 and b10). (c) TAMRA-loaded SNs from WT, APP, or Tau mice were used to determine the astrocytic uptake. TAMRA positive astrocytes were quantified by flow cytometry after different incubation times (c1). The curves were adjusted to a one-phase association kinetic and the calculated half-time constants were represented (c2). Data are mean± SD of six experiments. Significant differences in TAMRA uptake (c1) were calculated using two-way ANOVA followed by Bonferroni post hoc test (F (2,92) = 59.71, $p < .0001$; *$p < .05$). Half-time differences (c2) were assessed using one-way ANOVA (F(2,15) = 31.32, $p < .0001$) and Tukey post hoc test ($p < .05$). (d) Astrocytes were incubated (6 hr) with pHRodo labeled SNs, washed and positive cells were quantified by flow cytometry at different times (d1, chase). The number of pHRodo positive cells were normalized using the data at the initial 6 hr time. Curves were fitted to one-phase dissociation kinetic and the half-time constants were represented (d2). Data are mean ± SD of seven (SNs-WT) or four (SNs-APP, SNs-Tau) independent experiments. Significant differences were calculated using two-way ANOVA (d1, chase times F(2,76) = 21.27, $p < .00001$;) or one-way ANOVA (d2, half-time constants F(2,12) = 13.51, $p < .0001$) followed by Bonferroni or Tukey post hoc test. *$p < .05$. Scale bars, b1–b3 and b4–b6, 30 µm; b7, 2 µm; b8, 0.2 µm; b9, 1 µm; b10, 0.5 µm [Color figure can be viewed at wileyonlinelibrary.com]

described by the osmium fixation, dehydration and embedding steps. The primary antibody was omitted in negative control experiments. Samples for conventional electron microscopy and those processed with the immunogold technique, were visualized first using semithin sections stained with toluidine blue and then selected areas were cut in ultrathin sections and examined with an electron microscope (JEOL JEM 1400).

2.12 | Statistical analysis

Statistical analyses were performed using the GraphPad software 7.0. Data are presented individually or as mean ± standard deviation (SD). The comparison between two groups was done by two-tailed Student´s t test. Data with more than two groups were analyzed using one-way ANOVA, followed by Tukey post hoc test. Data with two independent factors were analyzed using two-way ANOVA, followed by Bonferroni post hoc test. The significance was always set at 95% of confidence.

3 | RESULTS

3.1 | Deficient phagocytosis and degradation of Abeta-containing dystrophic synapses by astrocytes

The phagocytic capacity of astrocytes was assayed using primary cultures from WT mice and synaptoneurosomes (SNs), isolated from 12-month-old APP (amyloidopathy model), 9-month-old Tau-P301S (tauopathy model) or 12-month-old WT (controls) mice. SNs preparations contained pre- and postsynaptic markers (such as synaptophysin, the glutamate vesicular transporter Vglut and the postsynaptic scaffold protein PSD95 in all three mice groups, Figure 1a,a1). Total (Tau46 or Tau12) and phosphorylated AT8 and AT100-positive Tau were specifically detected in SNs-Tau (Figure 1a,a2). As expected, APP-derived SNs, but not those derived from the WT or Tau mice, were positive for monomeric and oligomeric Abeta (6E10 + 82E1 positive) forms (Figure 1a,a3). Pathogenic proteins (phospho- or total Tau and Abeta) were absent in WT-derived SNs. Peri-plaque dystrophic neurites in APP mice, are predominantly composed of enlarged presynaptic elements, containing multiple vesicles of different origin but most of them from the autophagy-lysosomal pathway (Gomez-Arboledas et al., 2018; Sanchez-Varo et al., 2012; Trujillo-Estrada et al., 2014). Thus, we evaluated the presence of dystrophic structures in APP-derived SNs by EM (Figure S1a,a2,a3). Dystrophic-like structures were identified in APP-derived SNs, and were totally absent in the SNs fractions from WT mice (Figure S1a,a1). We also tested whether the APP-derived SNs fractions could be engulfed by primary astrocytes. As revealed by confocal double immunofluorescence labeling using anti-Abeta42 and anti-GFAP antibodies, Abeta-positive SNs were internalized by astrocytes after 6 hr of incubation (Figure 1b,b1–b6). This result was also confirmed by immunogold EM (Figure 1b,b7–b10). Abeta42 immunogold-positive phagocytic structures (phagosomes) were

found within primary astrocytes incubated with SNs derived from APP mice. Using these SNs preparations, we next quantitatively evaluated the astrocytic phagocytosis and degradative properties. SNs fractions (from WT, APP or Tau mice) were loaded with either TAMRA (uptake experiments; Figure S1b,c) or covalently labeled with the pH sensitive dye pHRodo (degradation kinetics, chase experiments, Figure S1d). Positive cells were quantified by flow cytometry. As shown (Figure 1c,c1), TAMRA-loaded WT- or Tau-derived SNs were efficiently and rapidly internalized by astrocytes. Data were fitted using one-phase association kinetic, and the "half-time" constants were calculated (Figure 1c,c2). No differences between SNs-WT and SNs-Tau were observed. However, in parallel experiments, SNs-APP presented a significantly slower kinetics (Figure 1c,c1) that, consequently, resulted in a significant increase in the uptake half-time constant (Figure 1c,c2, one-way ANOVA $F_{(2, 13)} = 21.89$; $p < .0001$; Tukey $p < .05$). This inhibitory effect in the phagocytic capacity was specific for astrocytes, since primary microglial cells displayed no uptake differences (half-time constants: 0.39 ± 0.05 hr, 0.46 ± 0.15 hr and 0.51 ± 0.10 hr, $n = 3$, for TAMRA-loaded SNs-WT, SNs-APP or SNs-Tau, respectively; Figure S2).

Next, we evaluated the degradation of the engulfed material using pHRodo-labeled SNs. Control experiments demonstrated that pHRodo positive cargo was internalized by astrocytes and located in acidic compartments (Figure S1d). Thus, astrocytes were "pulsed" for 6 hr with pHRodo-labeled SNs (from WT, APP, or Tau), washed and "chased" for different times. As shown (Figure 1d,d1), the number of pHRodo positive cells decreased over time, as expected from a degradative process. Similar to the previous data, astrocytes in presence of SNs-WT or SNs-Tau presented identical responses. In both cases, the number of pHRodo-positive cells showed a relatively fast decay kinetic that was fitted by a single mono-exponential function (see Figure 1d,d1,d2). By contrast, pHRodo-SNs from APP mice displayed inefficient degradation. In fact, the number of pHRodo-positive cells remained significantly elevated even after 48 hours of incubation. In consequence, the half-time constant for APP-derived SNs increased significantly ($p < .05$, Tukey), as compared with either WT or Tau derived SNs (one-way ANOVA $F_{(2,12)} = 13.51$, $p < .0001$; Figure 1d,d2).

The different degradation of engulfed APP- and WT or Tau-derived SNs was also assessed at the protein level. Synaptic proteins (synaptophysin or PSD95) from SNs were initially accumulated in astrocytes and eliminated in a time-dependent manner (Figure 2a,b). In fact, comparable decay constants were observed for both, WT or Tau-derived proteins, including total Tau (Figure 2a,b,c). Quantitatively, these data were similar to those observed using pHRodo (compare Figures 1d and 2b,c). On the other hand, and in consonance with our previous data, astrocytes loaded with SNs-APP accumulated synaptophysin, PSD95 and, more relevant, Abeta peptides. The quantitative analysis of these experiments (Figure 2b,c) demonstrated the existence of a significant increase in the decay constant for all APP-derived SNs proteins (one-way ANOVA $F_{(7, 26)} = 11.84$, $p < .001$; Tukey $p < .05$; Figure 2c). Thus, these data demonstrated that, at least in vitro, primary astrocytes presented clear deficiencies in the capacity
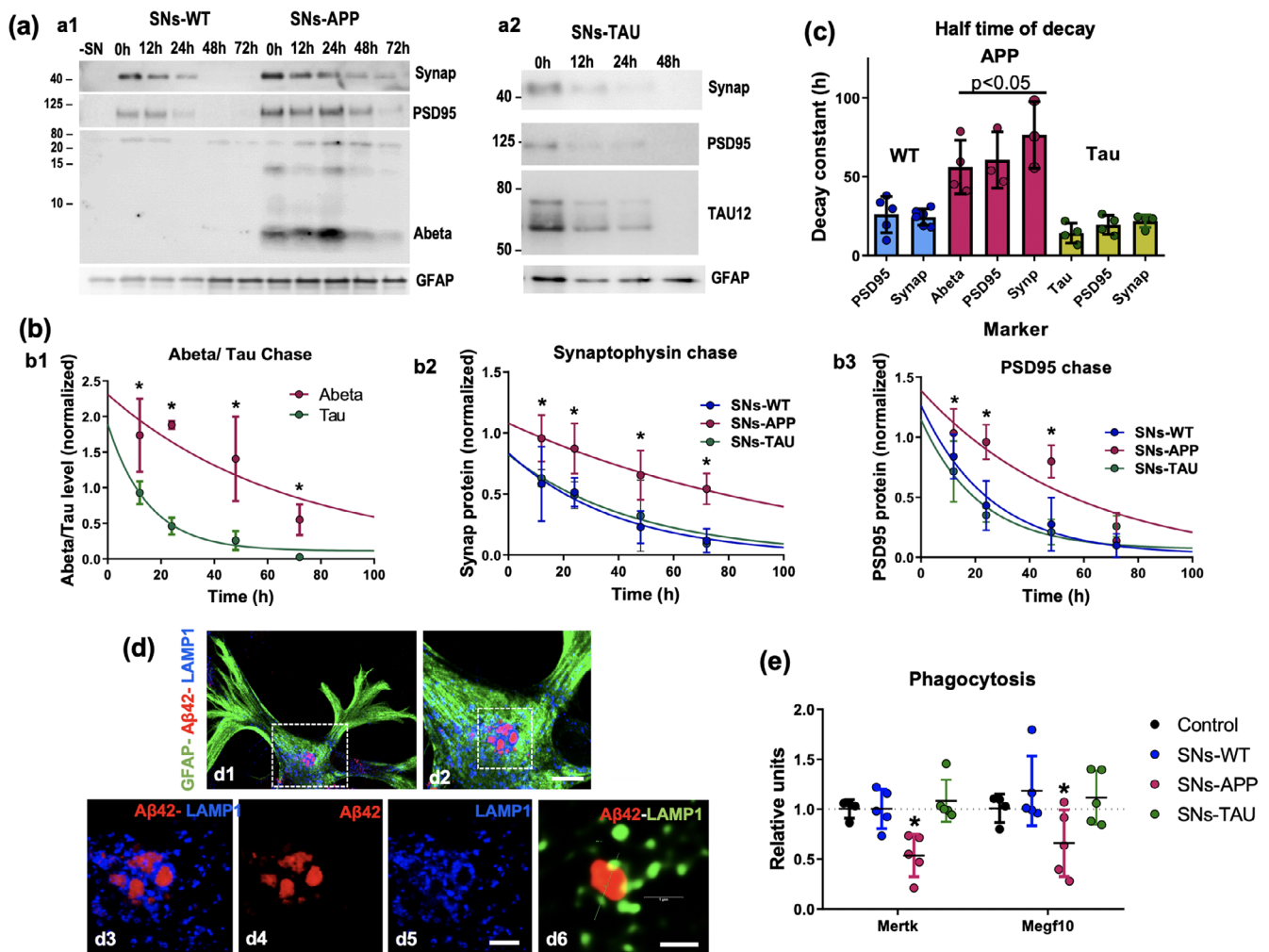
FIGURE 2 Reduction of the astrocytic degradative capacity of Abeta-containing SNs. (a) The time-dependent elimination of SN-derived proteins (synaptophysin, PSD-95, total Tau or Abeta) was assessed by Western-blots using total proteins isolated from astrocyte cultures. Representative Western blots are shown in a1 and a2. Control experiments, in absence of SNs, demonstrated the synaptoneurosomal origin of the different proteins (first lane in a1). (b) Quantitative analysis of Abeta or Tau (b1), synaptophysin (b2) and PSD-95 (b3) content within astrocytes. Data are mean ± SD of five (SNs-WT) or four (SNs-APP, SNs-Tau) independent experiments. Significant differences were calculated using two-way ANOVA (b1, $F_{(1,36)}$ = 83.32, $p < .0001$; b2, $F_{(2, 68)}$ = 16.33, $p < .0001$; b3, $F_{(2, 68)}$ = 22.73) followed by Bonferroni ($p < .05$ indicated in the figure). (c) Shown are the calculated half-time decay constants (from data in b). Significance was tested by one-way ANOVA ($F_{(7,26)}$ = 11.84. $p < .0001$), followed by Tukey post hoc test ($p < .05$). (d) Triple GFAP/Abeta42/Lamp1 confocal immunofluorescence of primary astrocytes (in green) incubated with SNs derived from APP mice revealed multiple Abeta-positive SNs (in red) within astrocytic cytoplasm (d1 and detail in d2). These SNs are surrounded by numerous lysosomes (in blue) but no fusion between both compartments is detected (see d3 to d5). Super-resolution image (d6) of an Abeta42-positive SN (in red) surrounded by Lamp1-positive lysosomes (in green) shows scarce overlap between these two structures. (e) Mertk and Megf10 expression was evaluated in astrocyte cultures ($n = 5$) treated, in parallel, with SNs isolated from WT, APP or Tau mice. Untreated cultures were used as controls. The expression of both phagocytic receptors decreased exclusively in SNs-APP, as compared with other groups (two-way ANOVA $F_{(3,30)}$ = 11.03, $p < .0001$; Bonferroni *$p < .05$). Scale bars, d1, 25 μm; d2, 10 μm; d3–d5, 5 μm; d6, 1 μm [Color figure can be viewed at wileyonlinelibrary.com]

to phagocytose and degrade SNs derived from APP mice, not noted in WT or Tau derived SNs.

The deficient degradation of APP-derived SNs internalized by primary astrocytes was also evidenced by confocal triple immunofluorescence of cultures after 24 hr of incubation (Figure 2d). Abeta42 labeled SNs accumulated within astrocytes (GFAP-positive), and did not co-localize with the lysosomal marker Lamp1 (Figure 2d,d1–d5). Lysosomes were located surrounding the engulfed SNs, however, only few partially contacted them (see Figure 2d,d6 using confocal super-

resolution microscopy). This may indicate deficient fusion of phagosomes with lysosomes, however, the mechanism precluding their interaction needs to be elucidated.

Since defective phagocytosis in astrocytes in a mouse model of septic shock has been described to be associated with a decrease in the expression of key genes implicated in the phagocytic process, such as Mertk and Mefg10 (Liddelow et al., 2017), we also tested the expression of these two genes. As shown in Figure 2e, their expression was unaltered (as compared with controls) in astrocytes treated
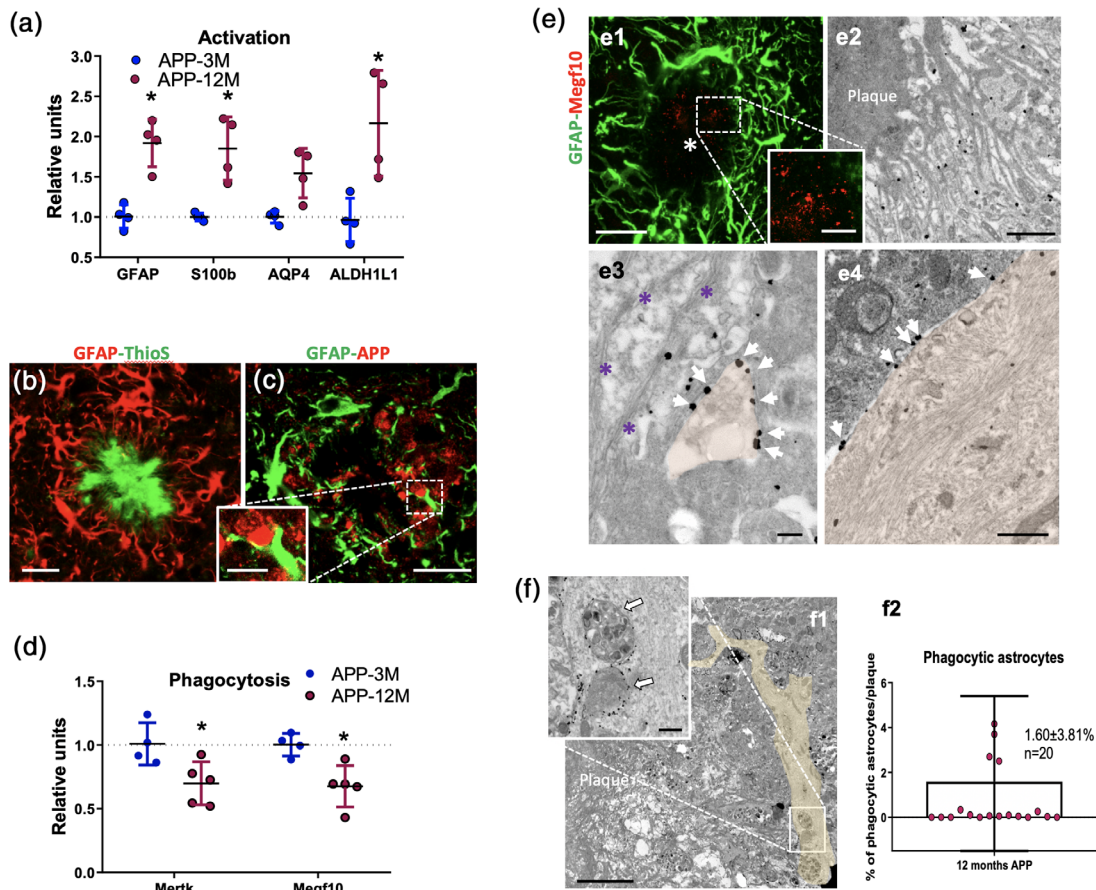
FIGURE 3 Limited phagocytic capacity of reactive astrocytes also in 12-month-old APP mice. (a) The expression of classical astrocytic gene markers (such as GFAP, S100b, Aqp4 or ALDH1L1) showed a significant increase (two-way ANOVA $F(1,24) = 56.43$, $p < .0001$; Bonferroni post hoc test $p < .05$) in 12-month-old APP mice, as compared with the pre-pathology stage in 3-month-old APP mice ($n = 4$/age). (b) Combined confocal GFAP immunofluorescence and thioflavin-S staining in 12-month-old APP mice showing a fibrillar Abeta plaque (green) surrounded by reactive astrocytes (red). (c) Double GFAP/APP confocal immunofluorescence in 12-month-old APP mice revealed the intimate contact of reactive astrocytic processes (green) with peri-plaque dystrophic neurites (red); a higher magnification detail is showed in the insert. (d) Expression analysis of Mertk and Megf10 genes in 3- and 12-month-old hippocampal APP samples ($F(1,14) = 19.32$, $p = .0006$, followed by Bonferroni post hoc test *$p < .05$). (e) Megf10 is expressed by thin distal reactive astrocyte processes in close contact with Abeta fibers from the periphery of Abeta plaques of 12-month-old APP mice; e1, double GFAP/Megf10 confocal immunofluorescence showing abundant reactive astrocytes processes (in green) around an Abeta plaque (not stained; indicated with asterisk); Megf10 does not colocalize with the GFAP-positive processes; instead, the labeling is mostly present in the plaque periphery. e2–e4; Megf10 immunogold electron microscopy precisely identified the location of Megf10 labeling (white arrows in e3 and e4) in the plasma membrane of thin astrocytic processes in contact with Abeta fibers (asterisk in e3). (f) Aquaporin 4 (AQP4) immunogold electron microscopy (f1) in 12-month-old APP mice showing a process (highlighted in yellow) from a reactive astrocyte near an Abeta plaque that contains several dystrophic neurites in the cytoplasm (arrows in the higher magnification detail in the inset). AQP4 labeling is located in the astrocytic plasma membrane, surrounding the internalized dystrophic neurites. Astrocytes containing dystrophies were quantified in 12-month-old APP mice and the percentages of positive astrocytes were calculated (f2, $n = 20$ plaques from 3 different animals). Scale bars, b and c, 20 μm (inset 5 μm); e1, 20 μm (inset 5 μm); e2, 1 μm; 3, 0.2 μm; e4, 0.5 μm; f1, 5 μm (inset, 0.5 μm) [Color figure can be viewed at wileyonlinelibrary.com]

with SNs from WT or Tau mice and significantly reduced in astrocytes treated with SNs-APP (two-way ANOVA $F(3,30) = 11.03$, $p = .0002$; Bonferroni $p < .05$).

3.2 | Limited astrocytic phagocytosis in aged APP mice

So far, our data demonstrated that SNs isolated from APP mice impaired the astrocyte capacity to engulf and degrade synaptic/

dystrophic elements in vitro. Therefore, we next aimed to verify this finding in vivo, in the hippocampus of 12-month-old APP model. As expected, astrocytes were reactive, as shown by the upregulated expression of pan-astrocytic proteins GFAP, S100b, ALDH1L1 (Figure 3a, two-way ANOVA $F(1,24) = 56.43$, $p < .0001$; Bonferroni $p < .05$, for 12-month-old APP mice ($n = 4$) versus 3-month-old APP ($n = 4$)) in astrocytes surrounding Abeta plaques (Figure 3b). Reactive astrocytic processes were in close contact with the peri-plaque APP-positive dystrophic neurites (Figure 3c and inset). Interestingly, we observed reduced expression of Mertk and Megf10 genes in

12-month-old APP mice (Figure 3d, two-way ANOVA $F(1,14) = 19.32$, $p = .0006$, Bonferroni $p < .05$, $n = 4/5$ for 3 or 12 months old, respectively). The expression of Megf10 in the hippocampus of 12-month-old APP mice was also tested by immunofluorescence confocal microscopy. As shown in Figure 3e (e1 and inset) a faint punctuate Megf10 immunolabeling was observed in the peri-plaque area, where the thin distal astrocyte processes (weak or negative for GFAP labeling) are located. To visualize the precise location of Megf10 labeling we used immunogold EM (Figure 3e,e2–e4). Megf10 immunoreactivity was located at the plasma membrane of astrocytic processes closely associated with bundles of amyloid fibrils radiating from plaque cores. However, no immunostaining was observed in astrocytic processes in contact with axonal dystrophies. Furthermore, quantitative analysis of EM experiments (Figure 3f) of 12-month-old APP mice demonstrated that only $1.60 \pm 3.81\%$ ($n = 20$ plaques from three different animals) of the astrocytes directly contacting Abeta plaques displayed engulfed dystrophies within their cytoplasm. That is, astrocytes might also present, in vivo, limited phagocytic capacity of dystrophic elements. In addition, the ultrastructural analysis of reactive astrocytes in tagged APP mice showed the presence of partially digested inclusions (see Figure S3), suggesting also reduced degradative capacity.

3.3 | What causes inefficient phagocytosis in astrocytes? Abeta versus microglia

So far, our results demonstrated limited capacity of astrocytes to engulf and degrade Abeta-containing synapses including dystrophic presynaptic elements. This fact could be due to a direct action of Abeta or an indirect effect of microglial factors since: (a) microglia are present in vivo as well as in the primary astrocyte cultures (see below), and (b) it has been reported that astrocytes incubated with a cocktail of microglial cytokines, mimicking a septic shock milieu, show defective pHRodo uptake in vitro (Liddelow et al., 2017).

To evaluate the cross-talk between microglia and astrocytes, we first examined whether genes induced by microglial factors (septic-shock like astrocytic phenotype; Liddelow et al., 2017) such as *Gbp2*, *Ggta*, *Psmb8*, *Srgn*, *Gbln*, *H2-d1*, *H2-t23*, and *Serping* were up-regulated in cultured astrocytes exposed to SNs from WT, tauopathy or amyloidopathy mice, as well as in APP mice. Importantly, these genes were also up-regulated in astrocytes isolated from APP/PS1 mice (Orre et al., 2014), further supporting their relevance in AD. As shown (Figure 4a), the expression of microglia-dependent genes was slightly or not altered in astrocytes incubated in presence of WT- or Tau-derived SNs. By contrast, APP-derived SNs produced a significant increase in the expression of most of the microglia-dependent genes (Figure 4a; Control, WT- Tau- and APP-group comparison, two-way ANOVA $F(3,88) = 49.82$ $p < .0001$; Bonferroni $p < .05$; Control, WT-Tau- and APP-group gene expression, two-way ANOVA $F(7,88) = 4.45$; $p = .0003$; Bonferroni $p < .05$), with no significant alteration of genes independent from microglia (Figure 4b). On the other hand, considering that processes from reactive astrocytes are in close contact with the peri-plaque APP-positive dystrophic neurites

(Figure 3c and inset) and microglial cells (Gomez-Arboledas et al., 2018) in APP mice, it is plausible that reactive astrocytes express microglia-dependent markers. As shown in Figure 4c, the expression of 6 out 8 genes tested showed a significant increase in 12 months versus 3 months APP mice (two-way ANOVA $F(1,48) = 62.15$; Bonferroni $p < .05$, $n = 4$ per gene and age), whereas most microglia-independent genes were not altered in the same samples. Although we cannot rule out that microglia-dependent genes were expressed as well in cells other than astrocytes in vivo, taken together these data support a local influence of microglia in the phenotype of reactive astrocytes in AD.

On the other hand, in vivo reactive astrocytes are located surrounding Abeta plaques and, therefore, exposed to soluble oligomeric Abeta (oAbeta) peptides, released from the plaque periphery (Izuo et al., 2019; Sanchez-Varo et al., 2012; Serrano-Pozo et al., 2016). In consequence, soluble Abeta peptides may directly affect the phenotype of astrocytes in AD. Therefore, we next evaluated whether soluble oAbeta (S1 fractions) derived from 12-month-old APP-mice also exert a similar effect on primary cultures as APP-derived SNs.

As reported previously, the soluble S1 fractions, isolated from APP mice brain, contained Abeta oligomeric forms (see Jimenez et al., 2008; Kayed et al., 2003, 2007; Moreno-Gonzalez et al., 2009; Torres et al., 2012; Yang, Li, Xu, Walsh, & Selkoe, 2017). We corroborated the presence of soluble oAbeta in the S1 extracts (by dot blots and anti-oligomeric specific antibodies, that is, OC, fibrillar, and A11, prefibrillar oligomers). As shown (Figure 5a), S1 fractions from 12-month-old APP mice were enriched (as compared with age-matched WT) in OC- and A11-positive oligomers (protein loading controls were also showed in Figure 5a, lower panel). Thus, we next assessed, in vitro, whether treatment with S1 could affect the capacity of astrocytes to phagocytose and degrade WT-derived SNs. As shown (Figure 5b), the presence of S1 fractions produced a clear and significant inhibition of both TAMRA uptake (Figure 5b,b1, half-time constant comparison, two-tailed t test, $p < .05$, $n = 4$) and pHRodo decrease (Figure 5b,b2, $n = 3$). In fact, no decay in the number of pHRodo positive cells was observed in the time assessed, so no half-decay constant could be calculated. In any case, these data indicated that soluble S1 fractions produced a similar effect to that observed using intact APP-derived SNs.

As shown in Figure 5c,c1, extracellular soluble Abeta peptides induced an increase in the expression of 5 out 8 of the microglia-dependent genes (two-way ANOVA $F(2,83) = 172.40$, $p < .0001$; Bonferroni $p < .05$), whereas only 2 out of 8 microglia-independent genes were affected. Therefore, Abeta-containing SNs and soluble S1 fractions derived from APP mice produced a similar effect in astrocyte cultures. Although the data were compatible with a direct Abeta-mediated effect on both phagocytosis and expression of microglia-dependent genes in astrocytes, considering that $7.2 \pm 0.82\%$ ($n = 4$) of the total cells in the astrocyte cultures used were microglia, the possibility existed that the actions of Abeta on astrocytes were indirect, mediated by the activation of residual microglia.

In order to discriminate between direct and indirect effects of Abeta, we first tested whether an immortalized astrocyte cell line,
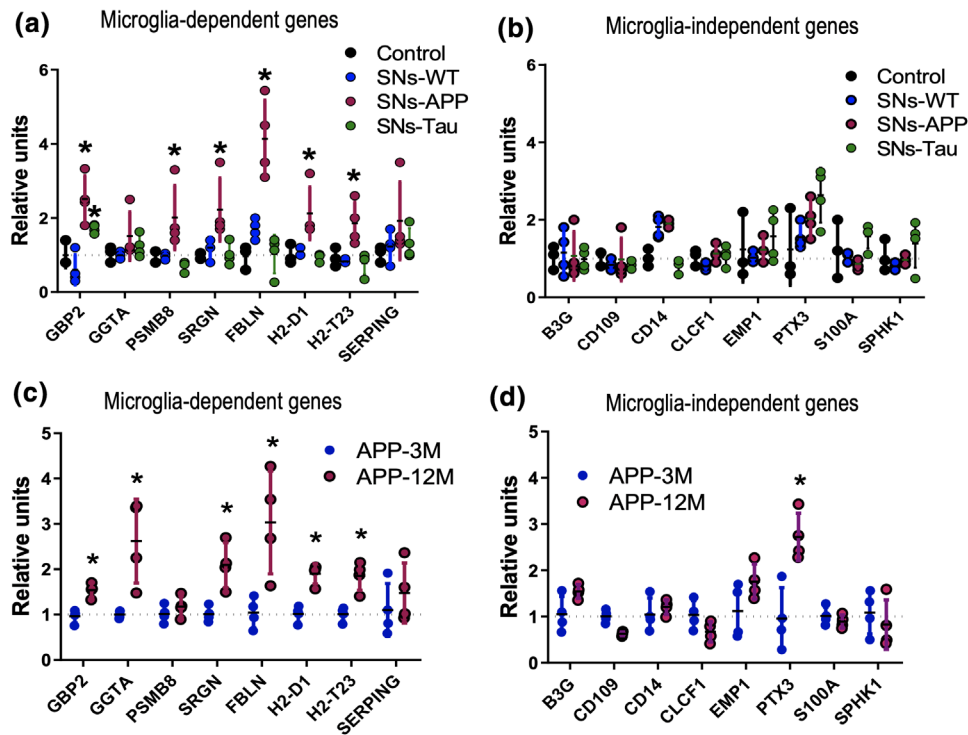
FIGURE 4 Increased expression of microglia-dependent genes in both SNs-APP treated astrocytes and 12-month-old APP hippocampus. The expression of microglia-dependent (a and c) and independent genes (b and d) was measured in astrocyte primary cultures (a and b) and in APP mice (c and d). (a, b) Astrocyte cultures (n = 4) were treated, in parallel, with SNs isolated from WT, APP or Tau mice. Untreated cultures were used as controls. Two-way ANOVA was used for comparison between different groups (microglia-dependent genes, two-way ANOVA F (3,88) = 39.73, p < .0001 and Bonferroni post hoc test; *p < .05). (c and d) Expression levels between hippocampal samples from 3- and 12-month-old APP mice were compared. Microglia-dependent and independent gene expression, two-way ANOVA F(1,48) = 62.15, p < .0001 or F(1,18) = 6.76, p = .01, respectively, Bonferroni post hoc test *p < .05 [Color figure can be viewed at wileyonlinelibrary.com]

WJE (Morikawa et al., 2005), presented similar deficiencies in SNs-APP phagocytic/degradative capacity (TAMRA- or pHRodo experiments) as the primary astrocyte cultures. Indeed, we observed an increase in the uptake half-time constant of SNs- APP, as compared with SNs-WT (0.53 ± 0.25 hr vs. 1.15 ± 0.29 hr, n = 5, p = .002 two tailed t test, for SNs-WT- or SNs-APP, respectively, Figure S4a). Also, in agreement with the observations in primary cultures, WJE-cells displayed a significant delay in the pHRodo degradation (7.59 ± 2.69 hr, n = 6, vs. 46.39 ± 15.82 hr, n = 4, of WT- and APP derived SNs, respectively; two tailed t test p = .004, Figure S4b). Therefore, even in absence of microglial cells, SNs from APP-mice caused significant impairment of astrocytic phagocytic/degradative capacity.

In a second set of experiments, contaminant microglial cells were eliminated using Clodronate liposomes (Kumamaru et al., 2012). After three days of treatment, only 0.63 ± 0.15% (n = 3) of total cells in the culture were from microglial origin (tested by flow cytometry). Using these astrocyte cultures virtually free from microglial contamination, we assessed the effect of APP-derived S1 fractions on pHRodo-labeled WT-SN uptake and degradation. As shown (Figure 5d), S1 fractions produced a clear inhibition in pHRodo-labeled WT-SNs uptake (first 24 hr incubation) and degradation in microglia-depleted cultures. In fact, no time-dependent decrease in the pHRodo positive

cells was detected and, in consequence, no half-decay constant could be calculated. Clodronate treated astrocytes (in absence of S1 fraction) efficiently phagocytosed and degraded SNs-WT (compared Figure 5b,b2,d). In consequence, the inhibition of the astrocytic phagocytosis was dependent on oAbeta and independent of microglia.

We also used microglial-free cultures to test the expression of microglia-dependent and independent genes (Figure 5c,c1,c2). Noteworthy, S1 fractions did not induce the expression of any of the tested genes in microglia-depleted astrocyte cultures (Figure 5c). These data suggest that the expression of these genes in astrocyte cultures contaminated with microglia was due to Abeta-mediated activation of microglial cells, whereas the deficiencies in either the uptake or degradation of APP-derived SNs were independent of microglia. Accordingly, S1 produced no effect on the expression of microglia-dependent genes in WJE cultures (Figure S4c).

Finally, we determined whether the effect of Abeta-containing S1 fractions in the expression of Mertk and Megf10 genes was also dependent on microglia (Figure 5e). The expression of these genes was consistently decreased in primary astrocytes treated with APP-derived SNs and in vivo in 12-month-old APP mice. In fact (Figure 5e), the expression of both genes was also significantly decreased in
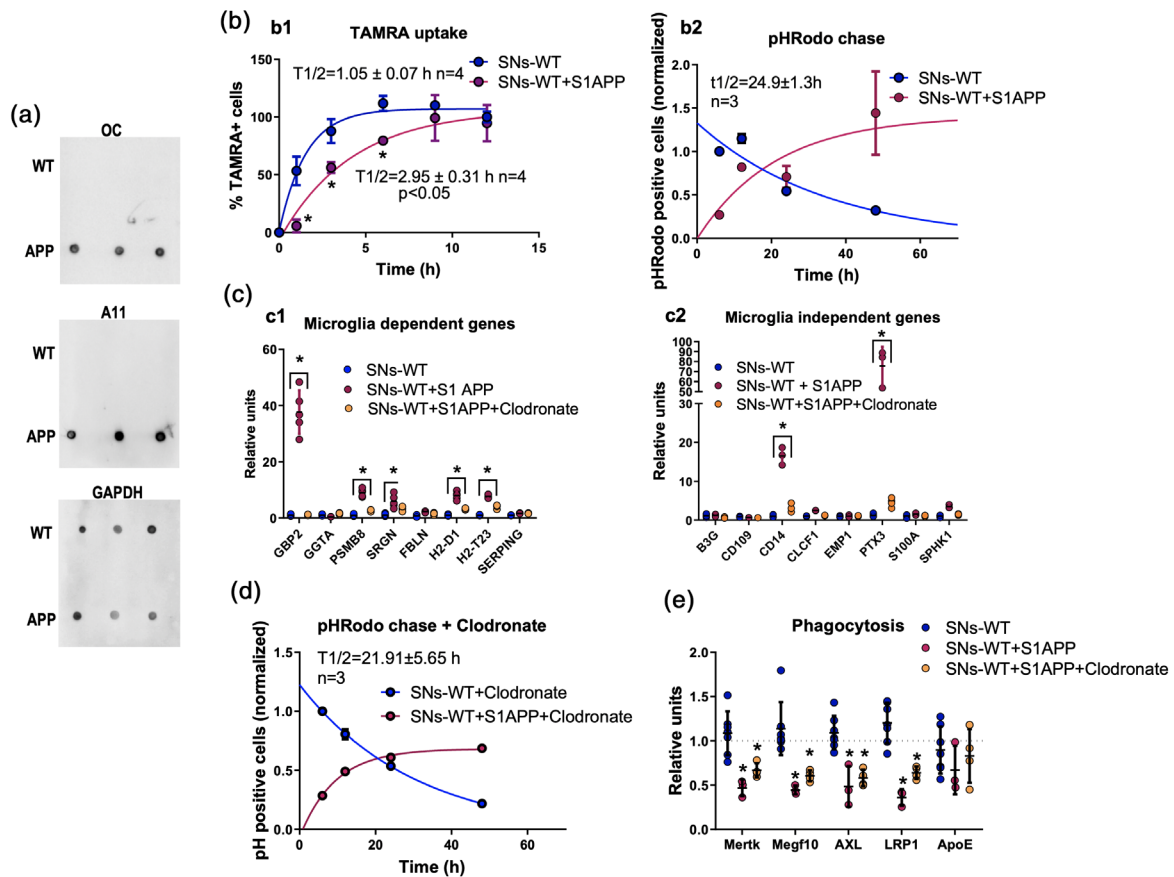
FIGURE 5 Microglia-independent inhibition of astrocytic phagocytosis by soluble (S1 fractions) oligomeric Abeta forms. (a) The presence of soluble Abeta oligomers was confirmed using dot blots and anti-oligomeric Abeta antibodies (OC and A11). Soluble proteins from 12-month-old WT or APP brains were doted (0.1 μg) and incubated with OC or A11. Parallel dots were incubated with anti-GAPDH as loading controls. (b) S1 fractions (10 μg/100 μl culture media) produced a clear inhibition of WT-SNs uptake (b1) or degradation (b2), as compared with untreated controls. TAMRA uptake and pHRodo chase experiments were analyzed as described in Figure 1. Half-time constants are shown in the figure. Data are means ± _SD_, _n_ = 4. Significance between the different time points was analyzed using two-way ANOVA ($F_{(1,36)}$ = 63.28, _p_ < .0001, Bonferroni post hot test *_p_ < .05) in b1. Differences between half-time constants (TAMRA uptake) were compared using two tailed t test (_p_ < .05) and are indicated in the panel (c). Microglia-dependent and independent gene expression was induced by APP-derived S1 fractions, and was inhibited after microglial elimination using Clodronate liposomes. Significant differences between SNs-WT, SNs-WT + S1APP treated astrocytes, in the presence or in the absence of clodronate, were assessed by two-way ANOVA, followed Bonferroni post hoc test (microglia-dependent genes $F_{(2,83)}$ = 172.40, _p_ < .0001; microglia-independent genes $F_{(2,83)}$ = 127.1, _p_ < .0001) *_p_ < .05. (d) APP-derived S1 fractions inhibited both uptake and degradation of pHRodo-labeled SNs-WT in the absence of microglial cells. Microglia were eliminated with Clodronate liposomes and the uptake/degradative capacity of astrocytes was assessed using pHRodo labeled SNs-WT, in the presence or in the absence of APP-derived S1 fractions. Data are means ± _SD_ of four experiments. (e) S1 fractions reduced the expression of phagocytosis receptors in the presence or in the absence of microglial cells. The expression of phagocytic receptors (Mertk, Megf10, AXL, and LRP1) was quantified in astrocyte cultures treated with SNs-WT (_n_ = 6) and S1-APP (_n_ = 3) or S1-APP plus clodronate (_n_ = 4). Significant differences were determined by two-way ANOVA ($F_{(2,55)}$ = 48.96, _p_ < .00001) followed by Bonferroni post hoc test (*_p_ < .05) [Color figure can be viewed at wileyonlinelibrary.com]

S1-treated astrocytes. Similarly, AXL and LRP1 receptors were also downregulated in presence of SNs-WT + S1. Furthermore, even in Clodronate treated cultures, S1 fractions produced a significant decrease in the expression of all tested phagocytic receptors (two-way ANOVA $F_{(2,55)}$ = 48.96, _p_ < .0001; Bonferroni _p_ < .05). Therefore, Abeta induced a decrease in Mertk and Megf10 expression, and in other phagocytic receptors, independently from the presence of microglial cells. ApoE expression was not altered in any condition tested and used as internal control.

4 | DISCUSSION

Astrocyte reactivity is inherent to the AD pathology (Perez-Nievas & Serrano-Pozo, 2018). Reactive astrocytes are predominantly located at Abeta plaques (Serrano-Pozo et al., 2011), but the exact roles of these reactive astrocytes are currently unknown (Arranz & Strooper, 2019). Among many different physiological functions, evidence implicates astrocytes in phagocytic processes in the normal brain (Xiao et al., 2014). Here, we present evidence supporting our prediction based upon in vivo data in amyloidogenic mice and AD

brains (Gomez-Arboledas et al., 2018) that phagocytosis is impaired in peri-plaque astrocytes. Specifically, we show that SNs containing Abeta, isolated from 12-month-old APP mice, reduce both the phagocytosis and intracellular degradation of the SNs content (i.e. Abeta and synaptic proteins) in vitro, using primary astrocytes. Importantly, this inhibitory effect seems to be specific for Abeta-containing SNs, since other potentially toxic SNs, such as those derived from 9-month-old Tau-P301S mice containing total, AT8- and AT100-positive Tau, produced no alterations in SNs phagocytosis or degradation (as compared with SNs-WT). In addition, although astrocytes indeed become reactive around Abeta plaques in APP mice at 12 months of age, less than 2% of these reactive astrocytes present phagocytosed dystrophies in their cytoplasm. Thus, astrocytes in the presence of Abeta present limited phagocytic capacity of presynaptic/axonal dystrophies in vitro and in vivo. Among other reasons, defective phagocytosis might be a consequence of the decreased expression of genes encoding for Mertk and/or Megf10, phagocytic receptors that mediate the binding and/or engulfment recognition of target synapses or cells (Chung et al., 2013; Iram et al., 2016; Scheib, Sullivan, & Carter, 2012; Tremblay, Cookson, & Civiero, 2019). Both Mertk and Megf10 receptors are implicated in synapse elimination by astrocytes (Chung et al., 2013). In consonance with these findings, we found a significant decrease in the expression of both receptors in presence of Abeta, even in 12-month-old APP mice, which, moreover, showed discrete expression of Megf10 in reactive astrocytes surrounding Abeta plaques. In this sense, immunogold EM demonstrated that Megf10 was preferentially located in astrocyte processes in close contacts with Abeta plaque fibers, rather than in those engulfing dystrophies. Thus, not only the decrease in the expression, but also the preferential localization of Megf10 in astrocytes contacting Abeta fibers rather than with dystrophies, might explain the inefficiency of astrocytic phagocytosis of dystrophic neurites.

Abeta affected not only phagocytosis in astrocytes, but also their capacity to degrade phagocytosed materials. This defect was demonstrated using three independent approaches: pHRodo experiments, western blots of Abeta and synaptic proteins, and confocal immunofluorescence, which showed a clear decrease in the degradation of phagocytosed material exclusively when Abeta was present. Although not investigated in detail, we indeed observed the accumulation of lysosomal vesicles (Lamp1-positive) surrounding, but not fused to, Abeta-positive phagocytosed SNs. Confocal super-resolution analysis confirmed this observation and, more relevant, partially digested phagocytic vesicles were observed in APP astrocytes. Therefore, in vivo and in vivo evidence suggest that Abeta containing dystrophic synapses inhibit both phagocytosis and the ensuing degradation process in astrocytes. A similarly inefficient astrocytic Abeta degradation was reported previously (Söllvander et al., 2016).

It could be argued that the limited or insufficient phagocytic/degradative capacity just reflects the normal reduction of the phagocytosis by adult astrocytes. In fact, astrocytes are highly active removing synapses and neurons at early stages of brain development (Chung et al., 2015), whereas the phagocytic activity has been suggested to decrease in the adulthood (Chung et al., 2013). However, it has been recently reported that adult astrocytes may become highly phagocytic in CNS pathologies, such as brain ischemia (Morizawa et al., 2017), multiple sclerosis and Parkinson's disease, where astrocytes respectively phagocytose myelin (Ponath et al., 2017), alpha-synuclein and dopaminergic cells (Morales, Sanchez, Rodriguez-Sabate, & Rodriguez, 2017; Tremblay et al., 2019). In AD, our data point to impaired phagocytic capacity, which may be aggravated due to the expression of ApoE4, as recently demonstrated (Chung et al., 2016; Lin et al., 2018). Malfunctional astrocytes, together with dysfunctional microglial responses (Navarro et al., 2018; Sanchez-Mejias et al., 2016), may, in turn, contribute to the accumulation of presynaptic/axonal dystrophies in AD. This may, in turn, exacerbate progression of AD, because dystrophic neurites have been implicated in the accumulation of phosphorylated Tau protein (He et al., 2018; Sanchez-Varo et al., 2012; Torres et al., 2012) and in the initiation of Tau pathology (He et al., 2018). Along these lines, rapid progressive AD cases might be attributed, in part, to defective clearance of dystrophic neurites as a consequence of the reportedly inefficient astrocyte reactivity (Drummond et al., 2017). An important observation of the present study is that Abeta, but not Tau, impairs astrocyte phagocytosis. Thus, it is tempting to speculate that the reason why dystrophic neurites resulting from the damage inflicted by Abeta plaques to neurons are observed in APP mice, as reported here and in Gomez-Arboledas et al., 2018), but appear to be absent in Tau models (our unpublished results), is not just that there are no Abeta plaques in the latter, but also that astrocyte phagocytosis might be preserved in Tau models.

Finally, an important finding of the present study is that the deficient phagocytosis in AD by astrocytes is directly caused by Abeta, and not by microglia. It has been described that astrocytes exposed to a cocktail of microglia-released cytokines such as TNF-alpha and IL-1alpha, and the complement factor C1q, display, among other features, a reduction in phagocytosis and a decrease in Mertk and Megf10 expression (Liddelow et al., 2017). Since reactive astrocytes and microglia are both located in close contact with Abeta plaques, it is possible that Abeta (either monomeric and/or oligomeric) in senile plaques, or released from them, induced the production of those factors by the peri-plaque microglia. Indeed, we found induction of expression of microglia-dependent genes in three different conditions: in astrocytes exposed to APP-derived SNs; in 12-month-old APP transgenic mice, and in astrocytes in presence of APP-derived S1 soluble fractions (OC and A11 positive). The presence of Abeta oligomers is a constant in the three cases (Figures 1 and 4), as it is the presence of microglial cells, since our primary astrocyte cultures contain a 7% of them, and astrocytes and microglial cells are located together in Abeta plaques. Thus, the concomitant partial expression of microglia-dependent genes and decreased phagocytosis were compatible with an indirect effect of Abeta on astrocytes through reactive microglia. However, SNs-APP also produced the same effect in the immortalized astrocyte cell line WJE, in the absence of microglial cells. Moreover, microglia depletion abolished the observed Abeta-induced expression of microglia-dependent genes, while Abeta still inhibited both the phagocytosis and the degradative process in astrocytes and,

furthermore, reduced the expression of Mertk and Megf10 (and other phagocytosis receptors). Therefore, Abeta seems to have two different actions on astrocytes: a direct inhibition of phagocytosis, and the indirect induction of transcriptional programs through microglial cells. In support of the latter, the microglia-dependent genes are also overexpressed in astrocytes isolated from an AD transgenic model (Orre et al., 2014). These data suggest a similar cross-talk between microglia and astrocytes in AD and septic shock. We thus conclude that the acquisition of a distinct phenotype in peri-plaque astrocytes depends on multiple signals, including those from Abeta and local microglia. Further studies will clarify the cause of astrocyte malfunction in AD, and its consequences on the pathological and clinical hallmarks of the disease.

DATA AVAILABILITY STATEMENT

The data that support the findings of this study are available from the corresponding authors upon reasonable request.

ORCID

Elena Galea https://orcid.org/0000-0003-4537-9897
Antonia Gutierrez https://orcid.org/0000-0002-6264-6152
Javier Vitorica https://orcid.org/0000-0002-0641-7902

REFERENCES

Arranz, A. M., & Strooper, B. D. (2019). The role of astroglia in Alzheimer's disease: Pathophysiology and clinical implications. *The Lancet Neurology*, *18*(4), 406–414. https://doi.org/10.1016/S1474-4422(18)30490-3

Blanchard, V., Moussaoui, S., Czech, C., Touchet, N., Bonici, B., Planche, M., ... Pradier, L. (2003). Time sequence of maturation of dystrophic neurites associated with Aβ deposits in APP/PS1 transgenic mice. *Experimental Neurology*, *184*(1), 247–263. https://doi.org/10.1016/S0014-4886(03)00252-8

Chung, W.-S., Allen, N. J., & Eroglu, C. (2015). Astrocytes control synapse formation, function, and elimination. *Cold Spring Harbor Perspectives in Biology*, *7*(9), a020370. https://doi.org/10.1101/cshperspect.a020370

Chung, W.-S., Clarke, L. E., Wang, G. X., Stafford, B. K., Sher, A., Chakraborty, C., ... Barres, B. A. (2013). Astrocytes mediate synapse elimination through MEGF10 and MERTK pathways. *Nature*, *504* (7480), 394–400. https://doi.org/10.1038/nature12776

Chung, W.-S., Verghese, P. B., Chakraborty, C., Joung, J., Hyman, B. T., Ulrich, J. D., ... Barres, B. A. (2016). Novel allele-dependent role for APOE in controlling the rate of synapse pruning by astrocytes. *Proceedings of the National Academy of Sciences*, *113*(36), 10186–10191. https://doi.org/10.1073/pnas.1609896113

Clarke, L. E., & Barres, B. A. (2013). Emerging roles of astrocytes in neural circuit development. *Nature Reviews Neuroscience*, *14*(5), 311–321. https://doi.org/10.1038/nrn3484

Dansokho, C., & Heneka, M. T. (2018). Neuroinflammatory responses in Alzheimer's disease. *Journal of Neural Transmission*, *125*(5), 771–779. https://doi.org/10.1007/s00702-017-1831-7

Drummond, E., Nayak, S., Faustin, A., Pires, G., Hickman, R. A., Askenazi, M., ... Wisniewski, T. (2017). Proteomic differences in amyloid plaques in rapidly progressive and sporadic Alzheimer's disease. *Acta Neuropathologica*, *133*(6), 933–954. https://doi.org/10.1007/s00401-017-1691-0

Forner, S., Baglietto-Vargas, D., Martini, A. C., Trujillo-Estrada, L., & LaFerla, F. M. (2017). Synaptic impairment in Alzheimer's disease: A dysregulated symphony. *Trends in Neurosciences*, *40*(6), 347–357. https://doi.org/10.1016/j.tins.2017.04.002

Gomez-Arboledas, A., Davila, J. C., Sanchez-Mejias, E., Navarro, V., Nuñez-Diaz, C., Sanchez-Varo, R., ... Gutierrez, A. (2018). Phagocytic clearance of presynaptic dystrophies by reactive astrocytes in Alzheimer's disease. *Glia*, *66*(3), 637–653. https://doi.org/10.1002/glia.23270

Hane, F. T., Lee, B. Y., & Leonenko, Z. (2017). Recent progress in Alzheimer's disease research, part 1: Pathology. *Journal of Alzheimer's Disease*, *57*(1), 1–28. https://doi.org/10.3233/JAD-160882

He, Z., Guo, J. L., McBride, J. D., Narasimhan, S., Kim, H., Changolkar, L., ... Lee, V. M.-Y. (2018). Amyloid-β plaques enhance Alzheimer's brain tau-seeded pathologies by facilitating neuritic plaque tau aggregation. *Nature Medicine*, *24*(1), 29–38. https://doi.org/10.1038/nm.4443

Heneka, M. T., Carson, M. J., Khoury, J. E., Landreth, G. E., Brosseron, F., Feinstein, D. L., ... Kummer, M. P. (2015). Neuroinflammation in Alzheimer's disease. *The Lancet Neurology*, *14*(4), 388–405. https://doi.org/10.1016/S1474-4422(15)70016-5

Iram, T., Ramirez-Ortiz, Z., Byrne, M. H., Coleman, U. A., Kingery, N. D., Means, T. K., ... Khoury, J. E. (2016). Megf10 Is a receptor for C1Q that mediates clearance of apoptotic cells by astrocytes. *Journal of Neuroscience*, *36*(19), 5185–5192. https://doi.org/10.1523/JNEUROSCI.3850-15.2016

Izuo, N., Murakami, K., Fujihara, Y., Maeda, M., Saito, T., Saido, T. C., ... Shimizu, T. (2019). An App knock-in mouse inducing the formation of a toxic conformer of Aβ as a model for evaluating only oligomer-induced cognitive decline in Alzheimer's disease. *Biochemical and Biophysical Research Communications*, *515*(3), 462–467. https://doi.org/10.1016/j.bbrc.2019.05.131

Jimenez, S., Navarro, V., Moyano, J., Sanchez-Mico, M., Torres, M., Davila, J. C., ... Vitorica, J. (2014). Disruption of amyloid plaques integrity affects the soluble oligomers content from Alzheimer disease brains. *PLoS One*, *9*(12), e114041. https://doi.org/10.1371/journal.pone.0114041

Jimenez, S., Baglietto-Vargas, D., Caballero, C., Moreno-Gonzalez, I., Torres, M., Sanchez-Varo, R., ... Vitorica, J. (2008). Inflammatory response in the hippocampus of PS1M146L/APP751SL mouse model of Alzheimer's disease: Age-dependent switch in the microglial phenotype from alternative to classic. *Journal of Neuroscience*, *28*(45), 11650–11661. https://doi.org/10.1523/JNEUROSCI.3024-08.2008

Jones, R. S., Minogue, A. M., Connor, T. J., & Lynch, M. A. (2013). Amyloid-β-induced astrocytic phagocytosis is mediated by CD36, CD47 and RAGE. *Journal of Neuroimmune Pharmacology*, *8*(1), 301–311. https://doi.org/10.1007/s11481-012-9427-3

Kayed, R., Head, E., Sarsoza, F., Saing, T., Cotman, C. W., Necula, M., ... Glabe, C. G. (2007). Fibril specific, conformation dependent antibodies recognize a generic epitope common to amyloid fibrils and fibrillar

oligomers that is absent in prefibrillar oligomers. *Molecular Neurodegeneration*, 2(1), 18. https://doi.org/10.1186/1750-1326-2-18

Kayed, R., Head, E., Thompson, J. L., McIntire, T. M., Milton, S. C., Cotman, C. W., & Glabe, C. G. (2003). Common structure of soluble amyloid oligomers implies common mechanism of pathogenesis. *Science*, 300(5618), 486–489. https://doi.org/10.1126/science.1079469

Kraft, A. W., Hu, X., Yoon, H., Yan, P., Xiao, Q., Wang, Y., ... Lee, J.-M. (2013). Attenuating astrocyte activation accelerates plaque pathogenesis in APP/PS1 mice. *The FASEB Journal*, 27(1), 187–198. https://doi.org/10.1096/fj.12-208660

Kumamaru, H., Saiwai, H., Kobayakawa, K., Kubota, K., van Rooijen, N., Inoue, K., ... Okada, S. (2012). Liposomal clodronate selectively eliminates microglia from primary astrocyte cultures. *Journal of Neuroinflammation*, 9(1), 116. https://doi.org/10.1186/1742-2094-9-116

Laurent, C., Buée, L., & Blum, D. (2018). Tau and neuroinflammation: What impact for Alzheimer's disease and tauopathies? *Biomedical Journal*, 41(1), 21–33. https://doi.org/10.1016/j.bj.2018.01.003

Liddelow, S. A., Guttenplan, K. A., Clarke, L. E., Bennett, F. C., Bohlen, C. J., Schirmer, L., ... Barres, B. A. (2017). Neurotoxic reactive astrocytes are induced by activated microglia. *Nature*, 541(7638), 481–487. https://doi.org/10.1038/nature21029

Lin, Y.-T., Seo, J., Gao, F., Feldman, H. M., Wen, H.-L., Penney, J., ... Tsai, L.-H. (2018). APOE4 causes widespread molecular and cellular alterations associated with Alzheimer's disease phenotypes in human iPSC-derived brain cell types. *Neuron*, 98(6), 1141–1154.e7. https://doi.org/10.1016/j.neuron.2018.05.008

Liu, C., Cui, G., Zhu, M., Kang, X., & Guo, H. (2014). Neuroinflammation in Alzheimer's disease: Chemokines produced by astrocytes and chemokine receptors. *International Journal of Clinical and Experimental Pathology*, 7(12), 8342–8355.

Masters, C. L., Simms, G., Weinman, N. A., Multhaup, G., McDonald, B. L., & Beyreuther, K. (1985). Amyloid plaque core protein in Alzheimer disease and Down syndrome. *Proceedings of the National Academy of Sciences*, 82(12), 4245–4249. https://doi.org/10.1073/pnas.82.12.4245

Meyer-Luehmann, M., Spires-Jones, T. L., Prada, C., Garcia-Alloza, M., de Calignon, A., Rozkalne, A., ... Hyman, B. T. (2008). Rapid appearance and local toxicity of amyloid-β plaques in a mouse model of Alzheimer's disease. *Nature*, 451(7179), 720–724. https://doi.org/10.1038/nature06616

Morales, I., Sanchez, A., Rodriguez-Sabate, C., & Rodriguez, M. (2017). Striatal astrocytes engulf dopaminergic debris in Parkinson's disease: A study in an animal model. *PLOS ONE*, 12(10), e0185989. https://doi.org/10.1371/journal.pone.0185989

Moreno-Gonzalez, I., Baglietto-Vargas, D., Sanchez-Varo, R., Jimenez, S., Trujillo-Estrada, L., Sanchez-Mejias, E., ... Gutierrez, A. (2009). Extracellular Amyloid-β and Cytotoxic Glial Activation Induce Significant Entorhinal Neuron Loss in Young PS1 M146L/APP 751SL Mice. *Journal of Alzheimer's Disease*, 18(4), 755–776. https://doi.org/10.3233/JAD-2009-1192

Morikawa, M., Fryer, J. D., Sullivan, P. M., Christopher, E. A., Wahrle, S. E., DeMattos, R. B., ... Holtzman, D. M. (2005). Production and characterization of astrocyte-derived human apolipoprotein E isoforms from immortalized astrocytes and their interactions with amyloid-β. *Neurobiology of Disease*, 19(1), 66–76. https://doi.org/10.1016/j.nbd.2004.11.005

Morizawa, Y. M., Hirayama, Y., Ohno, N., Shibata, S., Shigetomi, E., Sui, Y., ... Koizumi, S. (2017). Reactive astrocytes function as phagocytes after brain ischemia via ABCA1-mediated pathway. *Nature Communications*, 8(1), 28. https://doi.org/10.1038/s41467-017-00037-1

Navarro, V., Sanchez-Mejias, E., Jimenez, S., Muñoz-Castro, C., Sanchez-Varo, R., Davila, J. C., ... Vitorica, J. (2018). Microglia in Alzheimer's disease: Activated, dysfunctional or degenerative. *Frontiers in Aging Neuroscience*, 10, 140. https://doi.org/10.3389/fnagi.2018.00140

Nixon, R. A. (2007). Autophagy, amyloidogenesis and Alzheimer disease. *Journal of Cell Science*, 120(23), 4081–4091. https://doi.org/10.1242/jcs.019265

Nixon, R. A., & Yang, D.-S. (2011). Autophagy failure in Alzheimer's disease—Locating the primary defect. *Neurobiology of Disease*, 43(1), 38–45. https://doi.org/10.1016/j.nbd.2011.01.021

Olabarria, M., Noristani, H. N., Verkhratsky, A., & Rodríguez, J. J. (2010). Concomitant astroglial atrophy and astrogliosis in a triple transgenic animal model of Alzheimer's disease. *Glia*, 58(7), 831–838. https://doi.org/10.1002/glia.20967

Orre, M., Kamphuis, W., Osborn, L. M., Jansen, A. H. P., Kooijman, L., Bossers, K., & Hol, E. M. (2014). Isolation of glia from Alzheimer's mice reveals inflammation and dysfunction. *Neurobiology of Aging*, 35(12), 2746–2760. https://doi.org/10.1016/j.neurobiolaging.2014.06.004

Osborn, L. M., Kamphuis, W., Wadman, W. J., & Hol, E. M. (2016). Astrogliosis: An integral player in the pathogenesis of Alzheimer's disease. *Progress in Neurobiology*, 144, 121–141. https://doi.org/10.1016/j.pneurobio.2016.01.001

Perez-Nievas, B. G., & Serrano-Pozo, A. (2018). Deciphering the Astrocyte Reaction in Alzheimer's Disease. *Frontiers in Aging Neuroscience*, 10, 114. https://doi.org/10.3389/fnagi.2018.00114

Ponath, G., Ramanan, S., Mubarak, M., Housley, W., Lee, S., Sahinkaya, F. R., ... Pitt, D. (2017). Myelin phagocytosis by astrocytes after myelin damage promotes lesion pathology. *Brain*, 140(2), 399–413. https://doi.org/10.1093/brain/aww298

Puighermanal, E., Biever, A., & Valjent, E. (2016). Synaptoneurosome Preparation from C57BL/6 Striata. *Bio-Protocol*, 6(4), e1735. https://doi.org/10.21769/BioProtoc.1735

Rodríguez, J. J., Olabarria, M., Chvatal, A., & Verkhratsky, A. (2009). Astroglia in dementia and Alzheimer's disease. *Cell Death & Differentiation*, 16(3), 378–385. https://doi.org/10.1038/cdd.2008.172

Romero-Molina, C., Navarro, V., Sanchez-Varo, R., Jimenez, S., Fernandez-Valenzuela, J. J., Sanchez-Mico, M. V., ... Vizuete, M. (2018). Distinct microglial responses in two transgenic murine models of TAU pathology. *Frontiers in Cellular Neuroscience*, 12, 421. https://doi.org/10.3389/fncel.2018.00421

Sanchez-Mejias, E., Navarro, V., Jimenez, S., Sanchez-Mico, M., Sanchez-Varo, R., Nuñez-Diaz, C., ... Vitorica, J. (2016). Soluble phospho-tau from Alzheimer's disease hippocampus drives microglial degeneration. *Acta Neuropathologica*, 132(6), 897–916. https://doi.org/10.1007/s00401-016-1630-5

Sanchez-Varo, R., Trujillo-Estrada, L., Sanchez-Mejias, E., Torres, M., Baglietto-Vargas, D., Moreno-Gonzalez, I., ... Gutierrez, A. (2012). Abnormal accumulation of autophagic vesicles correlates with axonal and synaptic pathology in young Alzheimer's mice hippocampus. *Acta Neuropathologica*, 123(1), 53–70. https://doi.org/10.1007/s00401-011-0896-x

Scheib, J. L., Sullivan, C. S., & Carter, B. D. (2012). Jedi-1 and MEGF10 signal engulfment of apoptotic neurons through the tyrosine kinase Syk. *Journal of Neuroscience*, 32(38), 13022–13031. https://doi.org/10.1523/JNEUROSCI.6350-11.2012

Serrano-Pozo, A., Betensky, R. A., Frosch, M. P., & Hyman, B. T. (2016). Plaque-associated local toxicity increases over the clinical course of Alzheimer disease. *The American Journal of Pathology*, 186(2), 375–384. https://doi.org/10.1016/j.ajpath.2015.10.010

Serrano-Pozo, A., Mielke, M. L., Gómez-Isla, T., Betensky, R. A., Growdon, J. H., Frosch, M. P., & Hyman, B. T. (2011). Reactive glia not only associates with plaques but also parallels tangles in Alzheimer's disease. *The American Journal of Pathology*, 179(3), 1373–1384. https://doi.org/10.1016/j.ajpath.2011.05.047

Söllvander, S., Nikitidou, E., Brolin, R., Söderberg, L., Sehlin, D., Lannfelt, L., & Erlandsson, A. (2016). Accumulation of amyloid-β by astrocytes result in enlarged endosomes and microvesicle-induced apoptosis of neurons. *Molecular Neurodegeneration*, 11(1), 38. https://doi.org/10.1186/s13024-016-0098-z

Spillantini, M. G., & Goedert, M. (2013). Tau pathology and neurodegeneration. *The Lancet Neurology*, *12*(6), 609–622. https://doi.org/10.1016/S1474-4422(13)70090-5

Torres, M., Jimenez, S., Sanchez-Varo, R., Navarro, V., Trujillo-Estrada, L., Sanchez-Mejias, E., ... Vitorica, J. (2012). Defective lysosomal proteolysis and axonal transport are early pathogenic events that worsen with age leading to increased APP metabolism and synaptic Abeta in transgenic APP/PS1 hippocampus. *Molecular Neurodegeneration*, *7*(1), 59. https://doi.org/10.1186/1750-1326-7-59

Tremblay, M.-E., Cookson, M. R., & Civiero, L. (2019). Glial phagocytic clearance in Parkinson's disease. *Molecular Neurodegeneration*, *14*(1), 16. https://doi.org/10.1186/s13024-019-0314-8

Trujillo-Estrada, L., Dávila, J. C., Sánchez-Mejias, E., Sánchez-Varo, R., Gomez-Arboledas, A., Vizuete, M., ... Gutiérrez, A. (2014). Early neuronal loss and axonal/presynaptic damage is associated with accelerated amyloid-β accumulation in AβPP/PS1 Alzheimer's disease mice subiculum. *Journal of Alzheimer's Disease*, *42*(2), 521–541. https://doi.org/10.3233/JAD-140495

Verkhratsky, A., Zorec, R., Rodríguez, J. J., & Parpura, V. (2016). Astroglia dynamics in ageing and Alzheimer's disease. *Current Opinion in Pharmacology*, *26*, 74–79. https://doi.org/10.1016/j.coph.2015.09.011

Wyss-Coray, T., Loike, J. D., Brionne, T. C., Lu, E., Anankov, R., Yan, F., ... Husemann, J. (2003). Adult mouse astrocytes degrade amyloid-β in vitro and in situ. *Nature Medicine*, *9*(4), 453–457. https://doi.org/10.1038/nm838

Xiao, Q., Yan, P., Ma, X., Liu, H., Perez, R., Zhu, A., ... Lee, J.-M. (2014). Enhancing astrocytic lysosome biogenesis facilitates A clearance and attenuates amyloid plaque pathogenesis. *Journal of Neuroscience*, *34*(29), 9607–9620. https://doi.org/10.1523/JNEUROSCI.3788-13.2014

Yang, T., Li, S., Xu, H., Walsh, D. M., & Selkoe, D. J. (2017). Large soluble oligomers of amyloid β-protein from Alzheimer brain are far less neuroactive than the smaller oligomers to which they dissociate. *Journal of Neuroscience*, *37*(1), 152–163. https://doi.org/10.1523/JNEUROSCI.1698-16.2016

Yoshiyama, Y., Higuchi, M., Zhang, B., Huang, S.-M., Iwata, N., Saido, T. C., ... Lee, V. M.-Y. (2007). Synapse loss and microglial activation precede tangles in a P301S tauopathy mouse model. *Neuron*, *53*(3), 337–351. https://doi.org/10.1016/j.neuron.2007.01.010

Zhang, F., & Jiang, L. (2015). Neuroinflammation in Alzheimer's disease. *Neuropsychiatric Disease and Treatment*, *11*, 243–256. https://doi.org/10.2147/NDT.S75546

SUPPORTING INFORMATION

Additional supporting information may be found online in the Supporting Information section at the end of this article.